Published in final edited form as:

Nature. 2018 August ; 560(7719): 484–488. doi:10.1038/s41586-018-0425-3.

Restoration of vision after de novo genesis of rod photoreceptors in mammalian retinas

Kai Yao[1], **Suo Qiu**[1,4], **Yanbin V. Wang**[5,7], **Silvia J.H. Park**[5], **Ethan J. Mohns**[6], **Bhupesh Mehta**[7,9], **Xinran Liu**[8], **Bo Chang**[10], **David Zenisek**[7,5], **Michael C. Crair**[6,5], **Jonathan B. Demb**[5,7], and **Bo Chen**[1,2,3,†]

[1]Department of Ophthalmology, Icahn School of Medicine at Mount Sinai, New York, NY 10029, USA

[2]Department of Neuroscience, Icahn School of Medicine at Mount Sinai, New York, NY 10029, USA

[3]Department of Developmental and Regenerative Biology, Icahn School of Medicine at Mount Sinai, New York, NY 10029, USA

[4]State Key Laboratory of Ophthalmology, Zhongshan Ophthalmic Center, Sun Yat-sen University, Guangzhou 510060, P. R. China

[5]Department of Ophthalmology and Visual Science, Yale University School of Medicine, New Haven, CT 06511, USA

[6]Department of Neuroscience, Yale University School of Medicine, New Haven, CT 06511, USA

[7]Department of Cellular and Molecular Physiology, Yale University School of Medicine, New Haven, CT06511, USA

[8]Department of Cell Biology, Center for Cellular and Molecular Imaging, Yale University School of Medicine, New Haven, CT 06511, USA

[9]Department of Biophysics, National Institute of Mental Health and Neuro Sciences, Banglore 560029, India

[10]The Jackson Laboratory, 600 Main Street, Bar Harbor, ME 04609, USA

Abstract

[†]To whom correspondence should be addressed. bo.chen@mssm.edu.
Correspondence and requests for materials should be addressed to B.C. (bo.chen@mssm.edu).

Author Contributions

K.Y. and S.Q. performed injections, immunohistochemistry, and imaging analysis. Y.V.W., S.H.P. and J.B.D. performed retinal ganglion cell recordings. E.J.M. and M.C.C. performed cortical recordings. B.M. and D.Z. performed calcium current recordings. X.L. performed transmission electron microscopy analysis. B. Chang provided *Gnat1*^{rd17}:*Gnat2*^{cpfl3} double mutant mice. B. Chen designed the study and wrote the paper with instrumental input from J.B.D.

The authors declare no competing financial interests.

Readers are welcome to comment on the online version of the paper.

In zebrafish, Müller glial cells (MGs) are a source of retinal stem cells that can replenish damaged retinal neurons and restore vision[1]. In mammals, however, MGs lack regenerative capability as they do not spontaneously re-enter the cell cycle to generate a population of stem/progenitor cells that differentiate into retinal neurons. The regenerative machinery may exist in the mammalian retina, however, as retinal injury can stimulate MG proliferation followed by limited neurogenesis[2–7]. The fundamental question remains whether MG-derived regeneration can be exploited to restore vision in mammalian retinas. Previously, we showed that gene transfer of β-catenin stimulates MG proliferation in the absence of injury in mouse retinas[8]. Here, we report that following gene transfer of β-catenin, cell-cycle-reactivated MGs can be reprogrammed into rod photoreceptors via a subsequent gene transfer of transcription factors that are essential for rod cell fate specification and determination. MG-derived rods restored visual responses in *Gnat1*^{rd17}:*Gnat2*^{cpfl3} double mutant mice, a model of congenital blindness[9,10], throughout the visual pathway from the retina to the primary visual cortex. Together, our results provide evidence of vision restoration after de novo MG-derived genesis of rod photoreceptors in mammalian retinas.

In cold-blooded vertebrates such as zebrafish, Müller glial cells (MGs) act as retinal stem cells that readily proliferate to replenish damaged retinal neurons, establishing a powerful self-repair mechanism[11–13]. In mammals, however, MGs lack regenerative capability as they do not spontaneously re-enter the cell cycle. Injuring the mammalian retina does activate the proliferation of MGs, but with limited neurogenesis[2–7], and the required injury is obviously counterproductive for regeneration as it massively kills retinal neurons. Furthermore, there has been no convincing evidence that MG-derived regeneration improves vision in mammals. To test whether MG-derived neurogenesis improves vision without the necessity for retinal injury, we reprogrammed MGs *in vivo* to generate new rod photoreceptors in mature mouse retinas. We previously reported that ShH10-GFAP-mediated gene transfer of β-catenin in MGs stimulates these cells to re-enter the cell cycle in the uninjured mouse retina[8]. To reprogram the cell-cycle-reactivated MGs into rod photoreceptors, we tested a combination of three transcription factors (Otx2, Crx, and Nrl) that are essential for determining rod cell fate during development[14–17].

In the developing mouse retina, generation of cell types completes by two postnatal weeks[18]. To examine whether new rod photoreceptors could be generated from MGs in the mature retina, we used a two-step reprogramming method to first stimulate MG proliferation by intravitreal injection of ShH10-GFAP-β-catenin at 4 weeks of age. This was followed two weeks later by a second injection of ShH10-GFAP-mediated gene transfer of *Otx2*, *Crx*, and *Nrl*. We first examined whether MGs could undergo successive rounds of cell division after the initial gene transfer of β-catenin. Following an EdU/BrdU double-labeling procedure developed to analyze the clonal expansion of horizontal cells[19], proliferating MGs were labeled with EdU at 10 days after the injection of ShH10-GFAP-β-catenin, and 24 hours later the S phase cells were labeled with BrdU. Retinas were harvested 4 days later to assay whether EdU$^+$ cells progressed through another cell division into a second round of S phase. Very few cells were co-labeled by EdU and BrdU (Extended Data Fig. 1), indicating that the vast majority of MGs undergo only one cell division after β-catenin gene transfer.

To identify MGs that may undergo rod photoreceptor differentiation after the second injection of ShH10-GFAP-mediated gene transfer of *Otx2*, *Crx*, and *Nrl*, we included in the first injection ShH10-Rhodopsin-tdTomato, a 2.1 kb rhodopsin promoter[20] driving the expression of tdTomato, together with ShH10-GFAP-GFP to label all transduced MGs (Fig. 1a). Based on morphological changes observed from different retinal samples after the second injection for rod induction, the progression of MG-derived rod differentiation was categorized into initial, intermediate, and terminal stages. At the initial stage, MGs turned on the expression of Rhodopsin-tdTomato, and the Rhodopsin-tdTomato$^+$ cells resembled MGs with the upper processes ending at the outer limiting membrane, and the lower processes (MG endfeet) extending to the nerve fiber layer (Fig. 1b–d). At the intermediate stage, there was an asymmetric cell division whereby the Rhodopsin-tdTomato$^+$ cell produced two daughter cells with different fates (Fig. 1e–g). One daughter cell apparently differentiated to a rod photoreceptor with its soma localized to the outer nuclear layer (ONL), and intriguingly, the MG-derived rod cell generated outer/inner segments, a specialized cellular structure essential for phototransduction. The second daughter cell remained in the inner nuclear layer (INL) with a typical MG morphology. At the terminal stage, the Rhodopsin-tdTomato$^+$ cell appeared to have differentiated to a mature rod, resembling native rods with outer/inner segments and an enlarged synaptic bouton-like terminal. The second daughter cell remained as a MG and shut off tdTomato expression, which itself was driven by the rod-specific rhodopsin promoter (Fig. 1h–j). MG-derived rod differentiation was observed throughout the treated retina, whereas no Rhodopsin-tdTomato$^+$ cells were observed in control retinas receiving the same treatments except that ShH10-GFAP-β-catenin was omitted from the first injection (Extended Data Fig. 2).

We quantified the progression of rod differentiation over time (1,000–1,200 Rhodopsin-tdTomato$^+$ cells, 6–8 retinas per time point; with additional examples in Extended Data Fig. 3). One week after the second injection (Fig. 1k), most Rhodopsin-tdTomato$^+$ cells (73.5%) were in the initial stage, with a smaller number in the intermediate (20.6%) and terminal stages (5.9%). Two weeks after the second injection (Fig. 1l), most Rhodopsin-tdTomato$^+$ (74.8%) were in the terminal stage. Four weeks after the second injection (Fig. 1m), nearly all Rhodopsin-tdTomato$^+$ cells were in the terminal stage (97.4%). The Rhodopsin-tdTomato$^+$ cells were positive for GFAP-GFP (Fig. 1e, h), indicating that they were indeed derived from MGs, as gene transfer using the ShH10 AAV serotype and GFAP gene promoter should selectively transduce MGs but not photoreceptors[8]. The expression of GFAP-GFP eventually turned off in MG-derived rods over time, and no GFP signal was detected in Rhodopsin-tdTomato$^+$ cells 12 weeks after the second injection (Extended Data Fig. 4). We also tested whether expression of *Otx2*, *Crx*, and *Nrl* individually or in pairs was sufficient for rod induction (Extended Data Fig. 5). Four weeks after the second injection, only with the combination of *Crx* and *Nrl* yielded Rhodopsin-tdTomato$^+$ cells, which were restricted to the initial stage of rod differentiation (Extended Data Fig. 6).

To trace the lineages of MGs following our two-step reprogramming method, we generated a MG fate mapping line (GFAP-Cre x Rosa26-tdTomato reporter line), which permanently labels MGs with tdTomato (Fig. 1n)[8]. MG fate mapping mice at 4 weeks of age were first injected with ShH10-GFAP-β-catenin to stimulate MG proliferation, followed two weeks later by ShH10-GFAP-mediated gene transfer of *Otx2*, *Crx*, and *Nrl* for rod induction. Four

weeks after the second injection, tdTomato$^+$ cells were observed in the ONL and appeared to have differentiated into mature rods with outer/inner segments (Fig. 1o), further demonstrating that the rod cells were derived from MGs in the treated retina. We occasionally observed MG-derived tdTomato$^+$ cells with a horizontal cell morphology (Extended Data Fig. 7), consistent with a role for *Otx2* in promoting the fate of both photoreceptors and horizontal cells[21].

To assess the efficiency of rod induction, we quantified the number of Rhodopsin-tdTomato$^+$ cells at 4 weeks after the second injection. Rhodopsin-tdTomato$^+$ cells were evenly distributed across the retina, with over 800 cells per mm^2 in each retinal quadrant (Fig. 1p–t). By contrast, no MG-derived rods were observed in control retinas (ShH10-GFAP-β-catenin omitted from the first injection) (Fig. 1t). We also examined regenerative capability of MGs in 7-month-old retinas. The production of Rhodopsin-tdTomato$^+$ cells was reduced to ~200 per mm^2 in each quadrant (Extended Data Fig. 8).

The rod consists of specialized structures for detection of photons and communication with downstream neurons. Using confocal microscopy and immunohistochemistry, we examined whether MG-derived rod cells expressed a set of rod genes (Rhodopsin, Gnat1/rod α-transducin, Peripherin-2, Recoverin, and Ribeye) that play important roles in the formation/maintenance of cellular structures and are essential for phototransduction. Wild-type mice at 4 weeks of age were first injected with ShH10-GFAP-β-catenin (stimulate MG proliferation) and ShH10-Rhodopsin-tdTomato (label MG-derived rods). Four weeks after the second injection for ShH10-GFAP-mediated gene transfer of *Otx2*, *Crx*, and *Nrl*, we observed that Rhodopsin-tdTomato$^+$ cells expressed Rhodopsin and Peripherin-2 in the outer segment (Fig. 2a–d, 2e–h), Gnat-1 and Recoverin in the soma and processes (Fig. 2i–l, 2m–p), and Ribeye in the synaptic terminal (Fig. 2q–t), which was enlarged to form a bouton in close apposition to the post-synaptic specialties of PKCα$^+$ rod bipolar cell dendrites (Fig. 2u–x). As the immunoreactivity for Rhodopsin and Peripherin-2 were present at high density and in close proximity to native rods, we confirmed the expression of both proteins in dissociated Rhodopsin-tdTomato$^+$ cells (Extended Data Fig. 9). The rod outer segment (ROS) consists of densely packed membrane discs housing essential proteins for phototransduction. The rod inner segment (RIS) is filled with long thin mitochondria providing a main energy source to meet the rod's high metabolic needs. Synthesized proteins and membranes are trafficked from the RIS to ROS via the connecting cilium (CC), a microtubule-based structure crucial for rod function and survival. Rods communicate with second-order neurons, bipolar and horizontal cells, through a highly specialized triad synaptic structure. Ultrastructural analysis using transmission electron microscopy showed that the MG-derived rods correctly formed the ROS (Fig. 2y), RIS (Fig. 2z), CC (Fig. 2z′ and 2z″), and classic triad synapse (Fig. 2z‴), which were morphologically similar to native rods.

To unambiguously assess the functionality of newly generated rod photoreceptors, we reprogrammed MGs in *Gnat1*^{rd17}:*Gnat2*^{cpfl3} double mutant mice, which lack photoreceptor-mediated light responses. Gnat1^{rd17} mice lack rod α-transducin, an essential component for phototransduction, and are a model of congenital stationary night blindness[9,22]. *Gnat2*^{cpfl3} homozygotes have mutated cone α-transducin, with poor cone-mediated responses evident by 3 weeks of age and complete lack of cone-mediated responses at 9 weeks of age[10].

Phototransduction occurs in the outer segment of photoreceptors. Light-driven translocation of Gnat1 allows rods to adapt over a wide range of light intensities[23], and also contributes to rod survival and synaptic transmission to rod bipolar cells[24]. To reconstitute phototransduction in MG-derived rods in *Gnat1*^{rd17}:*Gnat2*^{cpfl3} mice, we used ShH10-Rhodopsin-mediated gene transfer of the wild-type *Gnat1* in MGs. *Gnat1*^{rd17}:*Gnat2*^{cpfl3} mice at 4 weeks of age were first injected with ShH10-GFAP-β-catenin (stimulate MG proliferation), ShH10-Rhodopsin-tdTomato (label MG-derived rods), and ShH10-Rhodopsin-*Gnat1* (correct the Gnat mutation in MG-derived rods). Four weeks after the second injection for ShH10-GFAP-mediated gene transfer of *Otx2*, *Crx*, and *Nrl*, we observed that Gnat1 was localized to the ROS in the Rhodopsin-tdTomato^{+} MG-derived rods in dark-adapted retina (Fig. 3a). Following light stimulation (10,000 lux, 2 hours), Gnat1 translocated towards the inner retina to other cellular compartments including the RIS, soma, and synaptic terminal (Fig. 3d). However, the co-expressed Rhodopsin-tdTomato, which served as an internal control, distributed to all cellular compartments regardless of light stimulation (Fig. 3b, e). Furthermore, MG-derived rods were generated as effectively in *Gnat1*^{rd17}:*Gnat2*^{cpfl3} mice as those in wild-type mice (Fig. 3g–k). By contrast, no MG-derived rods were observed in control *Gnat1*^{r17}:*Gnat2*^{cpfl3} retinas (ShH10-GFAP-β-catenin omitted from the first injection) (Fig. 3k).

Vision is initiated by photoreceptors and propagated through synaptic transmission to bipolar cells. Synaptic release from rod photoreceptors requires a calcium current[25,26], which was examined in MG-derived rods (GFAP-GFP^{+} cells) with whole-cell voltage clamp recordings in a retinal slice preparation from *Gnat1*^{rd17}:*Gnat2*^{cpfl3} mice at 4 weeks after the second injection for rod induction. Prominent inward currents were recorded with a peak near 0 mV from treated retinas (Fig. 4a), consistent with the expected L-type calcium currents in rods[27].

Visual information is integrated by retinal ganglion cells (RGCs), the retina's output neurons. To examine whether MG-derived rods integrate into retinal circuits, we recorded light responses from RGCs of *Gnat1*^{rd17}:*Gnat2*^{cpfl3} mice at 4 weeks after the second injection for rod induction, using an *in vitro* preparation[28,29]. To distinguish rod- from cone-mediated responses, we targeted RGCs in the ventral retina, where cones primarily express UV-sensitive cone opsin, with peak sensitivity at 360 nm, whereas rods express rhodopsin with peak sensitivity at 500 nm[28,30]. Large somas in the ganglion cell layer were targeted for action potential recordings in response to green and UV light (1-mm diameter). In control retinas (ShH10-GFAP-β-catenin omitted from the first injection), RGCs lacked light responses (Fig. 4b, e, f); whereas about half of RGCs from treated retinas responded following either light onset (ON cells, n = 6; Fig. 4c) or light offset (OFF cells, n = 9; Fig. 4d, e, g). For the entire sample, RGCs from the treated retina showed stronger responses (18.0 +/− 3.6 spikes s^{-1}; mean +/− sem) to green light at an intermediate intensity compared to RGCs from the control retina (−0.03 +/− 0.76 spikes s^{-1}; Fig. 4e). For the responding RGCs (n = 15; Fig. 4e), the firing rate was ~3.5 times more sensitive to green light as compared to UV light (Fig. 4g), consistent with a rod-mediated response. The responding RGCs from treated retinas showed lower sensitivity than RGCs from wild-type (wt; C57BL/6 strain) retinas (Fig. 4h–k), especially for ON RGCs (Fig. 4i). For both ON and OFF RGCs, responses to a high light level in the treated retina resembled RGC responses to

a low light level in the wt retina (Fig. 4h, j), which is likely explained by the relatively smaller number of responsive rods in the treated retina.

We next tested whether RGC responses in the treated *Gnat1*^{rd17}:*Gnat2*^{cpfl3} mice could be transmitted to the primary visual cortex *in vivo*. Visually-evoked potentials (VEPs) were recorded in primary visual cortices of lightly-anesthetized *Gnat1*^{rd17}:*Gnat2*^{cpfl3} mice at 4 weeks after the second injection for rod induction from the treated and control (ShH10-GFAP-β-catenin omitted from the first injection) groups. VEPs were identified as negative deflections in the cortical local field potentials (LFPs) following stimulus onset. At the brightest intensity tested (3.2 $\log_{10}$ nW mm^{-2} at the retina; see Methods), the stimulus drove a distinctive response in the LFP of the treated group, while no response was recorded in the control group (Fig. 4l, m). The responses of the treated group were delayed and smaller relative to responses of C57BL/6 wt controls (Fig. 4l), perhaps explained by the cortical integration of relatively lower outputs from RGCs in the treated animals. Nevertheless, the significant post-stimulus LFP amplitudes from the treated mice confirmed rescued light response in the primary visual cortices in comparison to the control group (Fig. 4m).

Our results demonstrate that MGs, without retinal injury, can be reprogrammed *in vivo* to generate new rod photoreceptors that integrate into retinal circuits, and restore vision in mammals.

Methods

Animals

All procedures involving the use of animals in this study were approved by the Institutional Animal Care and Use Committees of the Icahn School of Medicine at Mount Sinai and Yale University. Wild-type mice (strain C57BL/6J) and Rosa26-tdTomato reporter mice (strain B6.Cg-Gt(ROSA)26Sor$^{tm14(CAG-tdTomato)Hze}$/J) were obtained from the Jackson Laboratory (Bar Harbor, ME). *Gnat1*^{rd17}:*Gnat2*^{cpfl3} double mutant mice were kindly provided by Dr. Bo Chang (The Jackson Laboratory, Bar Harbor, ME). For light adaptation, the mice were placed in the dark for at least 12 hours and the pupils were dilated with 1% tropicamide and 1% atropine before exposure to 10,000 lux white light for 2 hours. For dark adaptation, the mice were maintained in the dark for more than 12 hours and all procedures were performed under infrared illumination. Animals (males and females) were randomly assigned to groups. The sample size was chosen based on pilot studies for >80% power (R).

AAV production and intravitreal injection

cDNAs encoding GFP, tdTomato, β-Catenin, *Otx2*, *Crx* and *Nrl* were subcloned and inserted into a AAV vector backbone where the expression was driven by the GFAP promoter (a gift from Dr. Lin Tian at UC Davis), or the Rhodopsin promoter (subcloned from pRho-DsRed; Addgene #11156). The *Gnat1* cDNA, reversely transcribed and amplified from mouse retinal RNAs, was used to replace tdTomato in pAAV-Rho-tdTomato to build the pAAV-Rho-*Gnat1* vector. Individual Adeno-associated virus (AAV) was produced in HEK293T cells (ATCC, authenticated by AAV production and tested for mycoplasma contamination by PCR) by plasmid co-transfection and iodixanol gradient ultracentrifugation. Purified AAVs

were concentrated with Amicon Ultra-15 Filter Units (Millipore, Bedford, MA) to a final titer of 1.0–5.0 × 10^{13} genome copies/mL (Extended Data Table 1). Intravitreal injection was performed using a microsyringe equipped with a 33-gauge needle. The tip of the needle was passed through the sclera, at the equator and next to the dorsal limbus of the eye, into the vitreous cavity. Injection volume was 1 μl per eye for AAVs.

EdU and BrdU co-labeling and detection

EdU or BrdU solution (1 μL, 1 mg/mL) was intravitreally injected into the vitreous chamber. For BrdU detection, the retinas were rinsed with PBS after fixation with 4% paraformaldehyde and incubated with 2 M HCl for 30 min at room temperature. Rinse the retinas with PBS and incubate with a blocking buffer containing 5% normal donkey serum, 0.1% Triton X-100, and 0.1% NaN_3 in PBS for 2 hours at room temperature. Primary antibody for BrdU (Thermo Scientific) was added for overnight incubation at 4°C. Retinas were washed with PBS and incubated with secondary antibody (DyLight™594-conjugated AffiniPure Donkey Anti-Mouse IgG, Jackson ImmunoResearch) for 2 hours at room temperature. Analysis of EdU incorporation was performed using Click-iT EdU Kit (Thermo Scientific). EdU detection components were re-suspended according to manufacturer's instructions and applied directly to retinal samples. In brief, the solution for each EdU reaction has a total volume of 250 μl composed of 215 μl 1X Click-iT reaction buffer, 10 μl CuSO4, 0.6 μl Alexa Fluor azide, and 25 μl 1X Reaction buffer additive. After incubation in the reaction solution for 30 min at room temperature, samples were washed with PBS and mounted with Fluoromount-G for detection.

Immunohistochemistry and Imaging

Retinas were fixed with 4% paraformaldehyde in PBS for 30 min at room temperature, and sectioned at 20-μm thickness. Sample slides were washed with PBS before incubation with a blocking buffer containing 5% normal donkey serum, 0.1% Triton X-100, and 0.1% NaN_3 in PBS for 2 hours at room temperature. Primary antibodies were added for overnight incubation at 4°C. Primary antibodies used: Rhodopsin (1:250, Thermo Scientific, MS-1233-P1), Peripherin-2 (1:500, Millipore, MABN293), Recoverin (1:500, Millipore, AB5585), Gnat1 (1:1000, Santa Cruz, sc-389), PKCα (1:100, Santa Cruz, sc-8393), and Ribeye (1:500, Synaptic Systems, 192103). Sections were washed with PBS and incubated with secondary antibodies (Jackson ImmunoResearch) for 2 hours at room temperature. Cell nuclei were counterstained with DAPI (Sigma). Confocal Images were acquired using a Zeiss LSM 510 EXCITER microscope.

Transmission electron microscopy

The whole eye was fixed in 2.5% gluteraldehyde and 2% paraformaldehyde in 0.1M sodium cacodylate buffer pH7.4 with for 1 hour at room temperature. After the cornea was removed, samples were postfixed in 1% osmium tetroxide for 1 hour, en bloc stained in 2% aqueous uranyl acetate for a further hour then rinsed, dehydrated in ethanol and propylene oxide and infiltrated with Embed 812 (Electron Microscopy Science). The blocks were hardened overnight at 60°C. 60-nm sections were cut with a Leica ultramicrotome and collected on formvar/carbon coated nickel grids. Grids were placed section side down on drops of 1% hydrogen peroxide for 5 minutes, blocked for nonspecific binding on 3% bovine serum

albumin in PBS containing 1% Triton-X for 30 minutes. Grids were incubated overnight as a primary antibody with either a rabbit anti-GFP (T. Südhof lab, Stanford University) at 1:200 or rabbit anti-TdTomato at 1:100 (Clontech, 632496), rinsed in buffer and then incubated with the secondary antibody 10 nm protein A gold (Utrecht UMC) for 30 mins. The grids were well rinsed in PBS, fixed in 1% gluteraldehyde for 5 mins, rinsed again, dried and stained using 2% aqueous uranyl acetate and lead citrate. Sample grids were viewed using FEI Tencai Biotwin TEM at 80 kV of accelerating voltage. Images were acquired with a Morada CCD camera and iTEM (Olympus) software.

Mouse retinal slice preparation and calcium current recordings

Gnat1^{rd17}:*Gnat2*^{cpfl3} mice were anaesthetized with isoflurane (Sigma), sacrificed by cervical dislocation, and their eyes enucleated. Whole retinas were isolated and placed on a 0.45-μm cellulose acetate/nitrate membrane filter (Millipore), which was secured with vacuum grease to a glass slide adjacent to the recording chamber. Slices were cut to a thickness of 150 μm using a tissue slicer, and transferred to the recording chamber while remaining submerged. The recording chamber was immediately attached to a perfusion system, and the slices were perfused at a rate of 5 mL min^{-1} with Ames media bubbled with 95% O_2 and 5% CO_2. All stages of retinal preparation were carried out at room temperature in a dark room. The standard recording solution for regenerated rods was composed of (in mM): 108 gluconic acid, 5 EGTA, 10 CsCl, 10 TEA, 4 MgATP, 1 LiGTP. The pH was adjusted to 7.4 with CsOH. The osmolarity of both extracellular and intracellular solutions was 289–293, with a pH of 7.35–7.40.

Patch pipettes (tip resistance, 10 – 12 MΩ) were fabricated from borosilicate glass (TWF150-4, WPI) using a two-stage vertical puller (Narishige). Pipettes were coated with Sticky Wax, (Kerr Corp). Whole-cell recordings were obtained using a dual EPC10/2 amplifier (HEKA Instruments). Slices were viewed with a Zeiss Axioskop 2FS plus equipped with a water-immersion 40X DIC objective and using an infrared filter for illumination. Regenerated rods were identified by their shape, GFP fluorescence and position in the slice. Illumination for epifluorescence was performed using an X-Cite 120Q lamp (EXFO) with a 488 nm bandpass excitation filter set for imaging GFP fluorescence or 590 bandpass filter set for imaging RFP. Images were acquired before whole cell recording with Andor iXon camera controlled by a Shutter driver VCM-D1. Data were acquired using PatchMaster (HEKA Instruments), and analysis performed using Igor Pro (WaveMetrics) and Origin 7.5 (Microcal). Currents were elicited at 60-second intervals, collected at 20 kHz, and low-pass filtered at 1 kHz.

RGC recordings

Retinas from *Gnat1*^{rd17}:*Gnat2*^{cpfl3} double mutant mice were prepared as described previously (Wang et al., 2011; Ke et al., 2014). After dissecting the retina under infrared light, the tissue was superfused with Ames' medium bubbled with 95% O_2 and 5% CO_2 in a chamber on a microscope (Olympus BX51WI) stage at ~34 deg C. A patch pipette (tip resistance, ~3–5 MΩ) filled with Ames' medium was used to form a loose seal (~50–200 MΩ) on a large soma (>20-μm diameter) to record action potentials. Cells were targeted under microscopic control using infrared light, a 60X water objective lens (NA, 0.9) and an

infrared-sensitive camera (Retiga 1300, Qcapture software; Qimaging Corporation). Data were sampled at 10 kHz and recorded on a computer using a MultiClamp 700B amplifier and pClamp9 software (Molecular Devices).

A total of 12 animals were studied, six treated animals, four controls (i.e., beta-catenin delivery omitted from first virus injection) and two C57/B6 wildtype. Of these, six animals (three treated, three controls) were studied in a double blind fashion; the person performing the virus injection was not aware of the identity of the virus condition, and the person performing the recording did not know the treatment group of the animal until the conclusion of all experiments.

Light stimuli were 1-mm-diameter spots generated by green (peak, 530 nm) or ultraviolet (UV; peak, 370 nm) LEDs that were diffused and windowed by the aperture in the microscope's fluorescence port and projected through a 4X objective lens (NA, 0.13) onto the photoreceptor layer. In some experiments, light was attenuated with a 2.0 neutral density filter (NDF; Kodak Wratten, Edmund Optics) that attenuated green and UV light by 130- and 880-fold, respectively. Light was presented as 200-ms flashes on darkness every 10 secs. In one block of trials, green and UV light flashes were alternated for 10 levels, with increasing intensity over time. For some cells, the entire block was repeated both with and without the NDF in place. For some cells with weak or absent responses, light flashes were presented in the brighter range only. For cells with sensitive responses, flashes were presented either in the dimmer range only or in both ranges. Firing rate (spikes s^{-1}) was recorded during a response window (300–500 ms) and normalized by subtracting the average firing rate measured during baseline periods before (500 ms) and after the flash (500 ms, Fig. 4b–d). If there was an obvious response to either light onset or offset, the response window was adjusted accordingly (Fig. 4c, d). If there was not an obvious response, the window for light onset was used by default (Fig. 4b).

RGC responses were quantified by averaging firing rates for green flashes in the intensity range of −1.7 to −0.7 $\log_{10}$ nW/mm^2 (Fig. 4e), which included four flash levels for blocks with or without the NDF in place. From these averaged responses, we selected responding cells from the treated group that exceeded the largest response measured in the control group. For responding RGCs in the treated group, we averaged the response across cells and combined data over the dimmer and brighter stimulus ranges (Fig. 4g). We fit the flash intensity-response function using the equation:

$$R(I) = AI^q (I^q + \sigma^q)^{-1},$$

where I is intensity (nW mm^{-2}), A is the maximum response amplitude (spikes s^{-1}), σ is the intensity that drives a half-saturating response, and q determines the slope. Fitted sigmoidal curves (Fig. 4g) shared amplitude (A, 33.8 spikes s^{-1}) and exponent (q, 0.705) parameters but had unique semi-saturation constants (σ for green, −2.34 $\log_{10}$ nW mm^{-2}; σ for UV, −1.80 $\log_{10}$ nW mm^{-2}). Fitting was performed using least-squares routines in Matlab (Mathworks).

Visually-evoked potentials (VEPs) and multi-unit activity (MUA) recordings

Under isoflurane anesthesia (2%; Baxter, Deerfield IL), an injection of xylocaine/epinephrine (1.0%; AstraZeneca, Wilmington, DE) was delivered beneath the skin overlying the skull. The skull was then exposed, cleaned of tissue, and coated with a thin layer of cyanoacrylate adhesive (VetBond, 3M, St. Paul MN). A second layer of cyanoacrylate adhesive (Maxi-Cure, BSI, Atascadero CA) was used to attach 2 metal bars to the pretreated skull; these bars were then used to secure the head into a custom-built stereotaxic apparatus. A craniotomy was made over primary visual cortex, leaving the dura mater intact. Body temperature was maintained at 36°C during surgery and experiments via a heating pad placed below the subject. Pupils were dilated with 1% tropicamide and 1% atropine, and the eyes were then coated with a thin layer of silicone oil (Sigma, St. Louis MO) to prevent dehydration.

Neurophysiological signals were collected using a 16-site silicon probe with 4 recording sites on each of 4 shanks (100-μm vertical separation between recording sites; 125-μm horizontal spacing between shanks; 1–2-MΩ impedance; NeuroNexus Technologies, Ann Arbor MI). After the probe was lowered through the dura mater and into the cortex, a layer of agarose (1.5% in ACSF; Sigma) was applied to cover the craniotomy. An insulated silver wire (0.25-mm diameter; Medwire, Mt. Vernon NY) inserted above the cerebellum served as a reference electrode. Signals were preamplified 10x (MPA8I preamplifiers; Multi Channel Systems MCS GmbH, Reutlingen, Germany) before being amplified 200x and band-pass filtered at 0.3–5000 Hz (Model 3500; A–M Systems, Inc., Carlsborg, WA). The amplified and filtered signals were sampled at 25 kHz using a digital interface (Power 1401 mk 2; Cambridge Electronic Design, Cambridge, UK).

After the recording probe was implanted, isoflurane was lowered to 1.0–1.5% and mice were given 30 minutes to adapt to the dimly-lit testing area before visual stimuli were delivered. Stimuli were 50-ms flashes of white light from a light-emitting diode (LED) that was placed 1 cm from the eye. The LED had two peaks, at ~460 and ~550 nm, with an integrated intensity of ~20 μW mm^{-2}; taking into account the spectral tuning of Rhodopsin, this corresponded to an equivalent intensity at 500 nm (i.e., the peak sensitivity of Rhodopsin) of ~7.55 μW mm^{-2} at the cornea and ~1.42 μW mm^{-2} (or ~3.2 $\log^{10}$ nW mm^{-2}) on the retina (assuming a 4-mm^2 dilated pupil area and evenly-spread light over the ~21.2 mm^2 retinal area). Dimmer stimuli were also tested (1.2 and 2.8 $\log^{10}$ nW mm^{-2} on the retina). No response was observed to the dimmest intensity, whereas gradually stronger responses were observed to the two brighter intensities. Visually-evoked potentials were identified as negative deflections in the cortical local field potentials (LFPs) following stimulus onset, with greater negative amplitudes in deeper cortical layers than in superficial layers. For LFP analyses, the recording channel with the greatest negative amplitude in response to visual stimulation was used. Maximum negative deflections in the LFP during the 0.5 s following stimulus onset were measured, and, for each animal, we tested whether the median of the response distribution differed from zero (Wilcoxin signed-rank test). Analyses were performed using MATLAB (The MathWorks, Inc., Natick, MA), Spike2 (Cambridge Electronic Design) and GraphPad Prism 6 (GraphPad Software, San Diego, CA).

Statistical analysis

Statistical differences between different experimental groups were typically analyzed by a Student's t-test or one-way ANOVA test except in cases where the data were not normally distributed (e.g., LFP amplitudes), in which case a non-parametric test was used, as described above. Data are presented as mean ± SEM, except where data were skewed (e.g., LFP amplitudes), in which case a box plot indicates median ± inter-quartile range. A value of $p < 0.05$ is considered significant.

Data availability

The datasets generated and/or analysed during the current study are available from the corresponding author on reasonable request.

Extended Data

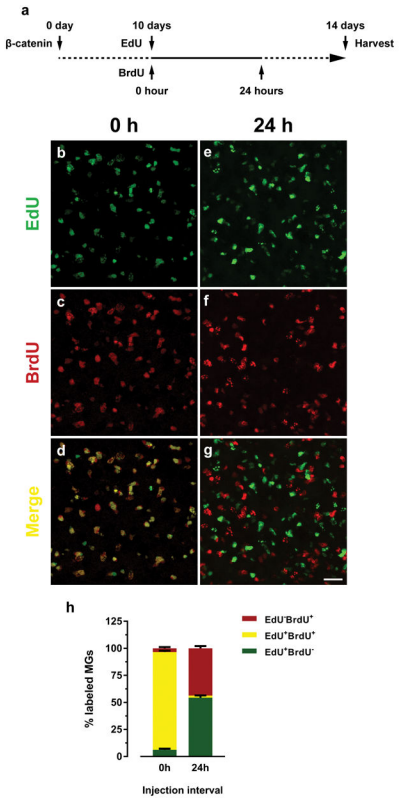

Extended Data Figure 1. MGs may undergo only one cell division after *β*-catenin gene transfer

a, A schematic illustration of EdU/BrdU double-labeling experiment. Wild-type retinas were injected with ShH10-GFAP-*β*-catenin (0 day), followed by an injection of EdU (10 days). BrdU was either co-injected with EdU (0 hour) or injected 24 hours after EdU injection (24 hours). Retinas were harvested 14 days after *β*-catenin gene transfer. **b–g,** Detection of EdU and BrdU labeled MGs. Scale bar: 20 μm. **h,** Percentage of MGs labeled by EdU (EdU $^{+}$BrdU^{-}, green), BrdU (red), or both (EdU^{+}BrdU^{+}, yellow). Experiments were repeated 3 times with similar results. Data are presented as mean ± SEM, n = 4 retinas.

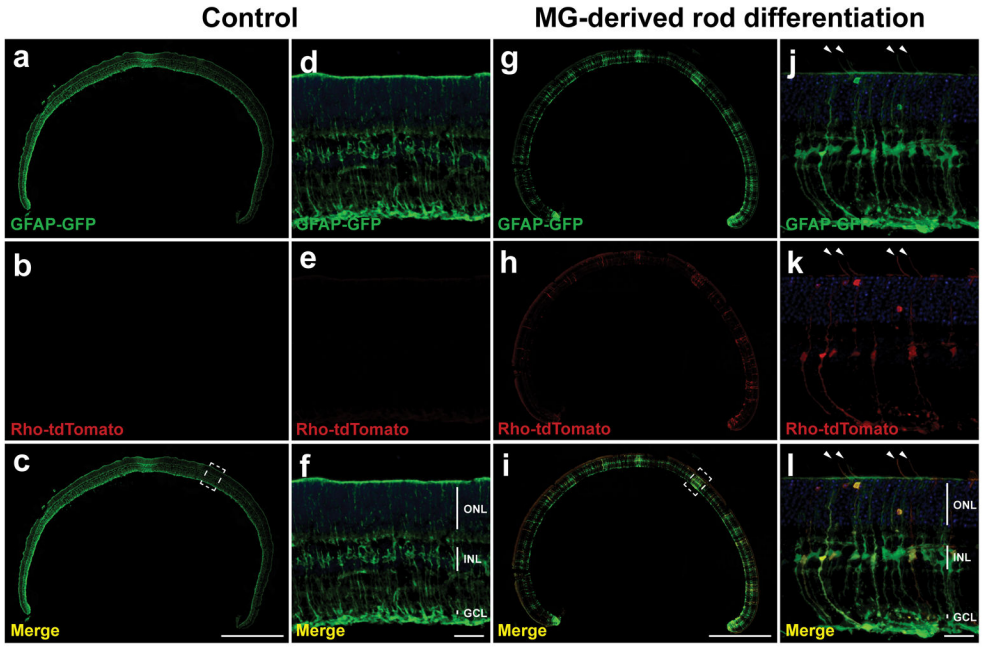

Extended Data Figure 2. MG-derived rod differentiation was observed across the whole retinal section

Wild-type retinas at 4 weeks of age were first injected with ShH10-GFAP-GFP (label transduced MGs), and ShH10-Rod-tdTomato (label MG-derived rods) in the absence (**a–f**) or presence (**g–l**) of ShH10-GFAP-β-catenin (stimulate MG proliferation), followed 2 weeks later by the second injection of ShH10-GFAP-mediated gene transfer of *Otx2*, *Crx* and *Nrl* for rod induction. Retinal samples were analyzed by confocal microscopy at 10 days after the second injection. The boxed areas in **c** and **i** are enlarged in **d–f** and **j–l**, respectively. Arrowheads: MG-derived rods. Scale bars: 750 μm in **a–c** and **g–i**; 25 μm in **d–f** and **j–l**. Experiments were repeated 4 times with similar results.

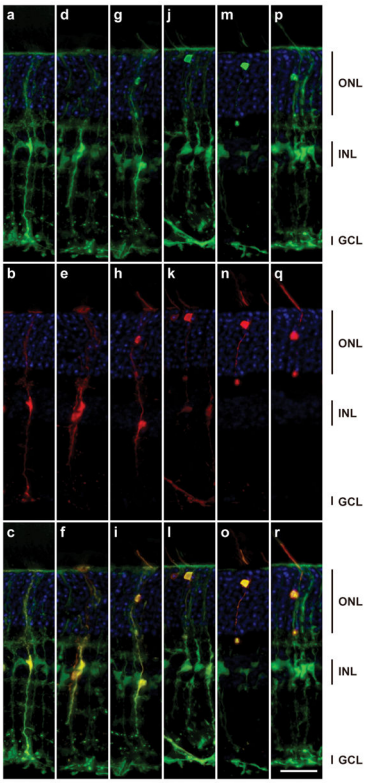

Extended Data Figure 3. Additional examples showing the progression of MG-derived rod differentiation

Wild-type retinas at 4 weeks of age were first injected with ShH10-GFAP-*β*-catenin, ShH10-GFAP-GFP, and ShH10-Rodopsin-tdTomato, followed 2 weeks later by the second injection of ShH10-GFAP-mediated gene transfer of *Otx2*, *Crx* and *Nrl* for rod induction. MG-derived rod differentiation progressed through the initial (**a–c**), intermediate (**d–f, g–i, j–l**) and terminal (**m–o, p–r**) stages. Scale bar: 25 μm. Experiments were repeated 6 times with similar results.

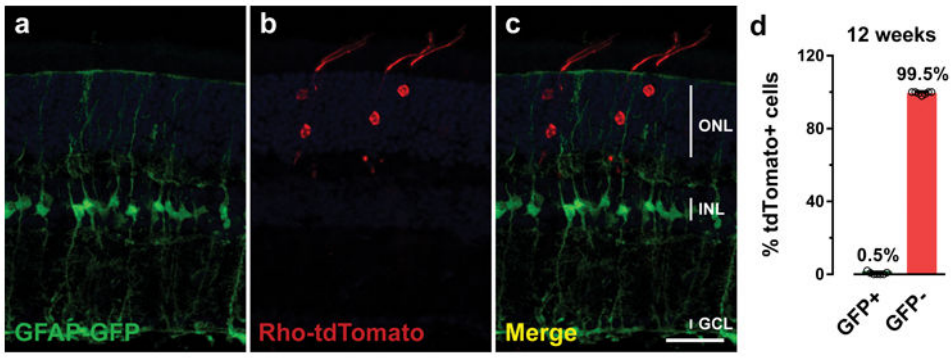

Extended Data Figure 4. MG-derived rods eventually turned off the expression of GFAP-GFP over time

Wild-type retinas at 4 weeks of age were first injected with ShH10-GFAP-*β*-catenin, ShH10-GFAP-GFP, and ShH10-Rhodopsin-tdTomato, followed 2 weeks later by the second injection of ShH10-GFAP-mediated gene transfer of *Otx2*, *Crx* and *Nrl* for rod induction. **a–**

c, Retinas were collected 12 weeks after the second injection and analyzed for the expression of GFAP-GFP in MG-derived rods labeled by Rhodopsin-tdTomato. Scale bar: 25 μm. Experiments were repeated 3 times independently with similar results. **d**, Percentage of Rhodopsin-tdTomato^{+} cells expressing GFAP-GFP. Data are presented as mean ± SEM, n = 7 retinas.

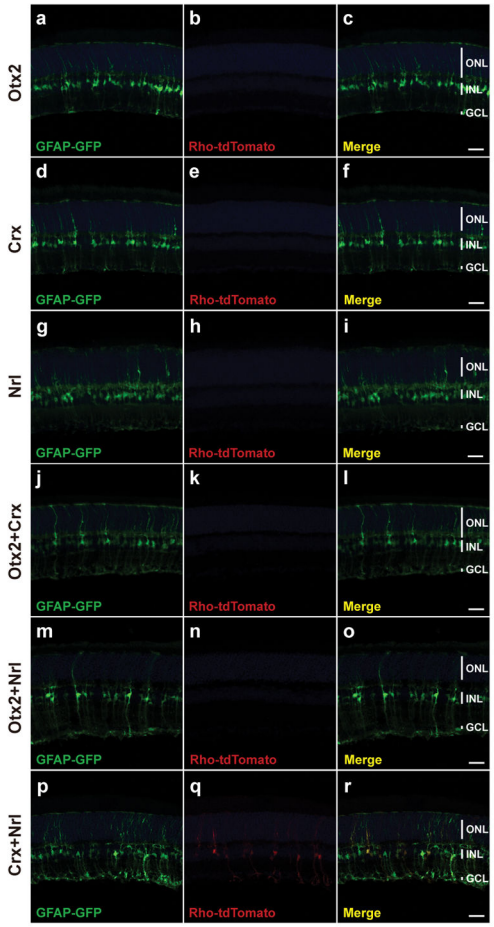

Extended Data Figure 5. Treatment with *Otx2*, *Crx*, and *Nrl* individually or in pairs is not sufficient for rod induction

Wild-type retinas were injected with ShH10-GFAP-*β*-catenin (MG proliferation), ShH10-GFAP-GFP (label transduced MGs), and ShH10-Rhodopsin-tdTomato (label MG-derived rods) at 4 weeks of age, followed 2 weeks later by the second injection of ShH10-GFAP-mediated gene transfer of transcription factors for rod induction. Samples were analyzed by confocal microscopy in retinal sections at 4 weeks after the second injection. **a–c,** *Otx2* treatment. **d–f,** *Crx* treatment. **g–i,** *Nrl* treatment. **j–l,** *Otx2*+*Crx* treatment. **m–o,** *Otx2*+*Nrl* treatment. **p–r,** *Crx*+*Nrl* treatment. Scale bar: 20 μm. Experiments were repeated 4 times with similar results.

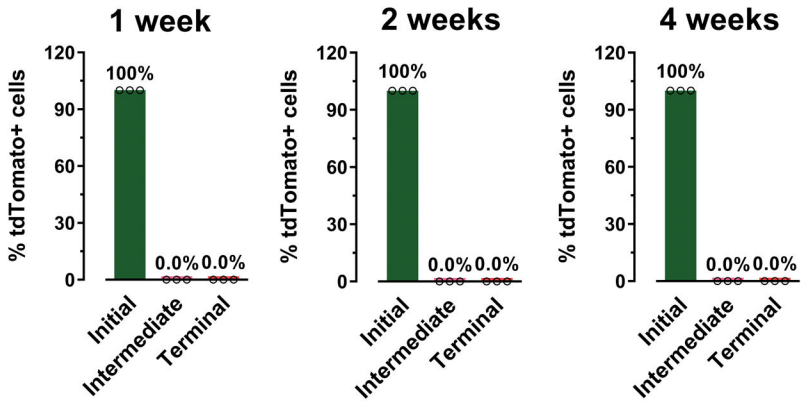

Extended Data Figure 6. Time course analysis of MG-derived rod differentiation in wild-type retinas treated with *Crx* and *Nrl*

Wild-type retinas at 4 weeks of age were first injected with ShH10-GFAP-*β*-catenin, ShH10-GFAP-GFP, and ShH10-Rhodopsin-tdTomato, followed 2 weeks later by the second injection of ShH10-GFAP-mediated gene transfer of *Crx* and *Nrl*. Rhodopsin-tdTomato^{+} cells were only detected in the initial stage of rod differentiation at 1, 2 and 4 weeks after the second injection. Data are presented as mean ± SEM, n = 3 retinas at each time point.

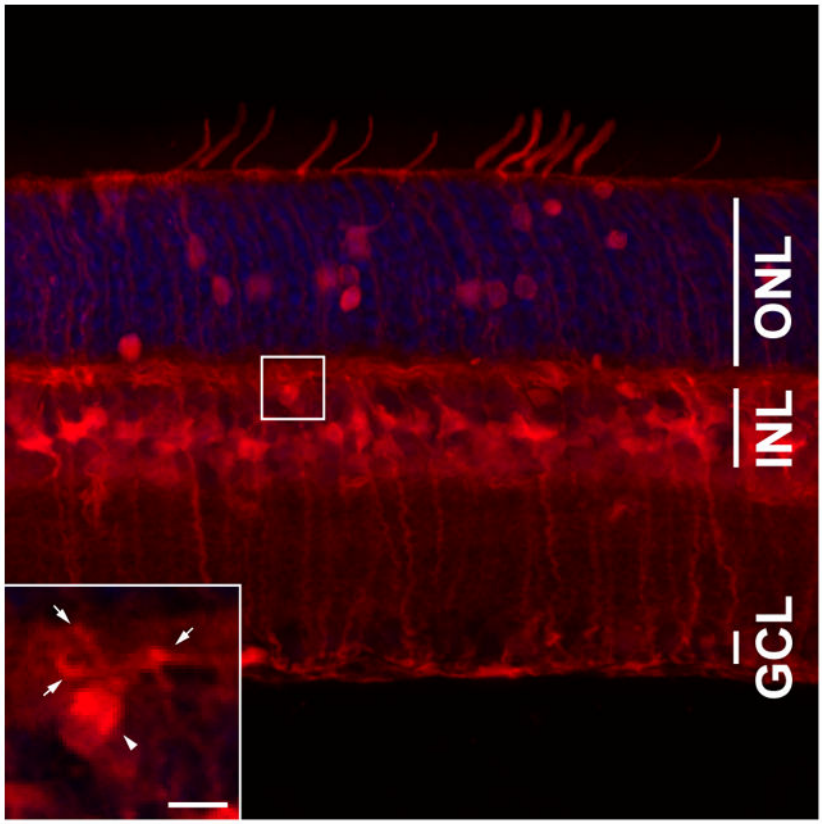

Extended Data Figure 7. Fate mapping experiments indicate that the two-step reprogramming method may occasionally produce cells with a horizontal cell morphology

The boxed area is enlarged to show an MG-derived tdTomato$^+$ cell with a horizontal cell morphology located in the outer region of the inner nuclear layer. Arrowhead: cell soma. Arrows: cell processes. Scale bar: 5 μm. Experiments were repeated 4 times with similar results.

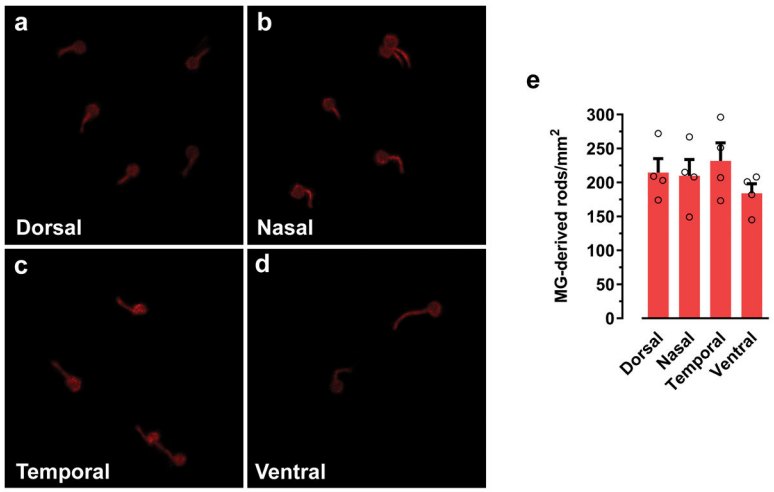

Extended Data Figure 8. MG-derived regeneration of rod photoreceptors decreases in aged mice

a–d, Generation of Rhodopsin-tdTomato$^+$ MG-derived rod photoreceptors in 7-month-old mouse retinas in the Dorsal (**a**), Nasal (**b**), Temporal (**c**), and Ventral (**d**) quadrants in retinal flat-mount preparations. Scale bar: 20 μm. Experiments were repeated 4 times with similar results. **e,** Quantification of Rhodopsin-tdTomato$^+$ MG-derived rods per mm^2 in the four retinal quadrants. Data are presented as mean ± SEM, n = 4 retinas.

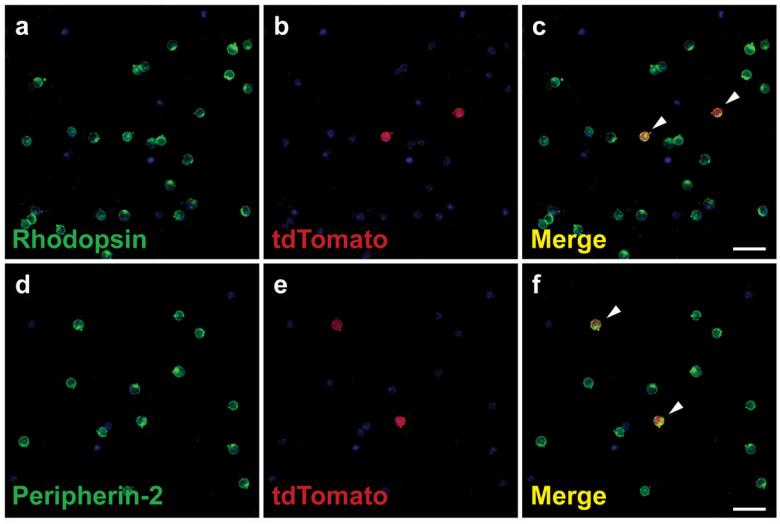

Extended Data Figure 9. MG-derived rod photoreceptors express Rhodopsin and Peripherin-2

Wild-type retinas were injected with ShH10-GFAP-β-catenin (MG proliferation) and ShH10-Rhodopsin-tdTomato (label MG-derived rods) at 4 weeks of age, followed 2 weeks later by the second injection of ShH10-GFAP-mediated gene transfer of *Otx2*, *Crx* and *Nrl*

for rod induction. Treated retinas were dissociated 4 weeks after the second injection and analyzed for the expression of Rhodopsin (**a–c**) and Peripherin-2 (**d–f**) using immunohistochemistry and confocal microscopy. Arrowheads: MG-derived rods were immunoreactive for Rhodopsin (**c**) and Peripherin-2 (**f**). Scale bar: 20 μm. Experiments were repeated 3 times with similar results.

Extended Data Table 1

Table of viral constructs, packaged viruses, and the virus titers after purification and concentration.

AAVs used in the study were purified, concentrated, and titered using quantitative real-time PCR.

Viral constructs	Virus	Titres
pAAV-GFAP-GFP	ShH10-GFAP-GFP	2.6×10^{13}
pAAV-GFAP-β-Catenin	ShH10-GFAP-β-Catenin	2.9×10^{13}
pAAV-Rho-tdTomato	ShH10-Rho-tdTomato	1.8×10^{13}
pAAV-GFAP-Otx2	ShH10-GFAP-Otx2	4.7×10^{13}
pAAV-GFAP-Crx	ShH10-GFAP-Crx	5.0×10^{13}
pAAV-GFAP-Nr1	ShH10-GFAP-Nr1	4.8×10^{13}
pAAV-Rho-Gnat1	ShH10-Rho-Gnat1	1.5×10^{13}

Acknowledgments

This research was supported by National Institutes of Health grants R01 EY024986, R01 EY021502, R01 EY014454, R01 EY021372, R01 EY015788, R01 EY023105, R01 EY021195, R01 EY014990, P30 EY026878, Pew Scholars Program in the Biomedical Sciences, Research to Prevent Blindness and the McGraw Family Foundation for Vision Research.

References

1. Goldman D. Muller glial cell reprogramming and retina regeneration. Nat Rev Neurosci. 2014; 15:431–442. nrn3723 [pii]. DOI: 10.1038/nrn3723 [PubMed: 24894585]
2. Elsaeidi F, et al. Notch Suppression Collaborates with Ascl1 and Lin28 to Unleash a Regenerative Response in Fish Retina, But Not in Mice. J Neurosci. 2018; 38:2246–2261. JNEUROSCI. 2126-17.2018 [pii]. DOI: 10.1523/JNEUROSCI.2126-17.2018 [PubMed: 29378863]
3. Jorstad NL, et al. Stimulation of functional neuronal regeneration from Muller glia in adult mice. Nature. 2017; 548:103–107. nature23283 [pii]. DOI: 10.1038/nature23283 [PubMed: 28746305]
4. Karl MO, et al. Stimulation of neural regeneration in the mouse retina. Proc Natl Acad Sci U S A. 2008; 105:19508–19513. 0807453105 [pii]. DOI: 10.1073/pnas.0807453105 [PubMed: 19033471]
5. Dyer MA, Cepko CL. Control of Muller glial cell proliferation and activation following retinal injury. Nat Neurosci. 2000; 3:873–880. DOI: 10.1038/78774 [PubMed: 10966617]
6. Ooto S, et al. Potential for neural regeneration after neurotoxic injury in the adult mammalian retina. Proc Natl Acad Sci U S A. 2004; 101:13654–13659. 0402129101 [pii]. DOI: 10.1073/pnas. 0402129101 [PubMed: 15353594]
7. Ueki Y, et al. Transgenic expression of the proneural transcription factor Ascl1 in Muller glia stimulates retinal regeneration in young mice. Proc Natl Acad Sci U S A. 2015; 112:13717–13722. 1510595112 [pii]. DOI: 10.1073/pnas.1510595112 [PubMed: 26483457]
8. Yao K, et al. Wnt Regulates Proliferation and Neurogenic Potential of Muller Glial Cells via a Lin28/let-7 miRNA-Dependent Pathway in Adult Mammalian Retinas. Cell Rep. 2016; 17:165–178. S2211-1247(16)31174-3 [pii]. DOI: 10.1016/j.celrep.2016.08.078 [PubMed: 27681429]

9. Calvert PD, et al. Phototransduction in transgenic mice after targeted deletion of the rod transducin alpha-subunit. Proc Natl Acad Sci U S A. 2000; 97:13913–13918. 250478897 [pii]. DOI: 10.1073/pnas.250478897 [PubMed: 11095744]
10. Chang B, et al. Cone photoreceptor function loss-3, a novel mouse model of achromatopsia due to a mutation in Gnat2. Invest Ophthalmol Vis Sci. 2006; 47:5017–5021. 47/11/5017 [pii]. DOI: 10.1167/iovs.05-1468 [PubMed: 17065522]
11. Fausett BV, Goldman D. A role for alpha1 tubulin-expressing Muller glia in regeneration of the injured zebrafish retina. J Neurosci. 2006; 26:6303–6313. 26/23/6303 [pii]. DOI: 10.1523/JNEUROSCI.0332-06.2006 [PubMed: 16763038]
12. Bernardos RL, Barthel LK, Meyers JR, Raymond PA. Late-stage neuronal progenitors in the retina are radial Muller glia that function as retinal stem cells. J Neurosci. 2007; 27:7028–7040. 27/26/7028 [pii]. DOI: 10.1523/JNEUROSCI.1624-07.2007 [PubMed: 17596452]
13. Fimbel SM, Montgomery JE, Burket CT, Hyde DR. Regeneration of inner retinal neurons after intravitreal injection of ouabain in zebrafish. J Neurosci. 2007; 27:1712–1724. 27/7/1712 [pii]. DOI: 10.1523/JNEUROSCI.5317-06.2007 [PubMed: 17301179]
14. Nishida A, et al. Otx2 homeobox gene controls retinal photoreceptor cell fate and pineal gland development. Nat Neurosci. 2003; 6:1255–1263. [PubMed: 14625556]
15. Chen S, et al. Crx, a novel Otx-like paired-homeodomain protein, binds to and transactivates photoreceptor cell-specific genes. Neuron. 1997; 19:1017–1030. [PubMed: 9390516]
16. Furukawa T, Morrow EM, Cepko CL. Crx, a novel otx-like homeobox gene, shows photoreceptor-specific expression and regulates photoreceptor differentiation. Cell. 1997; 91:531–541. [PubMed: 9390562]
17. Mears AJ, et al. Nrl is required for rod photoreceptor development. Nat Genet. 2001; 29:447–452. [PubMed: 11694879]
18. Livesey FJ, Cepko CL. Vertebrate neural cell-fate determination: lessons from the retina. Nat Rev Neurosci. 2001; 2:109–118. DOI: 10.1038/35053522 [PubMed: 11252990]
19. Ajioka I, et al. Differentiated horizontal interneurons clonally expand to form metastatic retinoblastoma in mice. Cell. 2007; 131:378–390. S0092-8674(07)01224-X [pii]. DOI: 10.1016/j.cell.2007.09.036 [PubMed: 17956737]
20. Matsuda T, Cepko CL. Electroporation and RNA interference in the rodent retina in vivo and in vitro. Proc Natl Acad Sci U S A. 2004; 101:16–22. [PubMed: 14603031]
21. Emerson MM, Surzenko N, Goetz JJ, Trimarchi J, Cepko CL. Otx2 and Onecut1 promote the fates of cone photoreceptors and horizontal cells and repress rod photoreceptors. Dev Cell. 2013; 26:59–72. S1534-5807(13)00344-4 [pii]. DOI: 10.1016/j.devcel.2013.06.005 [PubMed: 23867227]
22. Deng WT, et al. Functional interchangeability of rod and cone transducin alpha-subunits. Proc Natl Acad Sci U S A. 2009; 106:17681–17686. 0901382106 [pii]. DOI: 10.1073/pnas.0901382106 [PubMed: 19815523]
23. Sokolov M, et al. Massive light-driven translocation of transducin between the two major compartments of rod cells: a novel mechanism of light adaptation. Neuron. 2002; 34:95–106. S0896627302006360 [pii]. [PubMed: 11931744]
24. Majumder A, et al. Transducin translocation contributes to rod survival and enhances synaptic transmission from rods to rod bipolar cells. Proc Natl Acad Sci U S A. 2013; 110:12468–12473. 1222666110 [pii]. DOI: 10.1073/pnas.1222666110 [PubMed: 23836670]
25. Schmitz Y, Witkovsky P. Dependence of photoreceptor glutamate release on a dihydropyridine-sensitive calcium channel. Neuroscience. 1997; 78:1209–1216. S0306452296006781 [pii]. [PubMed: 9174087]
26. Thoreson WB, Nitzan R, Miller RF. Reducing extracellular Cl− suppresses dihydropyridine-sensitive Ca2+ currents and synaptic transmission in amphibian photoreceptors. J Neurophysiol. 1997; 77:2175–2190. [PubMed: 9114264]
27. Corey DP, Dubinsky JM, Schwartz EA. The calcium current in inner segments of rods from the salamander (Ambystoma tigrinum) retina. J Physiol. 1984; 354:557–575. [PubMed: 6090654]
28. Wang YV, Weick M, Demb JB. Spectral and temporal sensitivity of cone-mediated responses in mouse retinal ganglion cells. J Neurosci. 2011; 31:7670–7681. 31/21/7670 [pii]. DOI: 10.1523/JNEUROSCI.0629-11.2011 [PubMed: 21613480]

29. Ke JB, et al. Adaptation to background light enables contrast coding at rod bipolar cell synapses. Neuron. 2014; 81:388–401. S0896-6273(13)01006-4 [pii]. DOI: 10.1016/j.neuron.2013.10.054 [PubMed: 24373883]

30. Nikonov SS, Kholodenko R, Lem J, Pugh EN Jr. Physiological features of the S- and M-cone photoreceptors of wild-type mice from single-cell recordings. J Gen Physiol. 2006; 127:359–374. jgp.200609490 [pii]. DOI: 10.1085/jgp.200609490 [PubMed: 16567464]

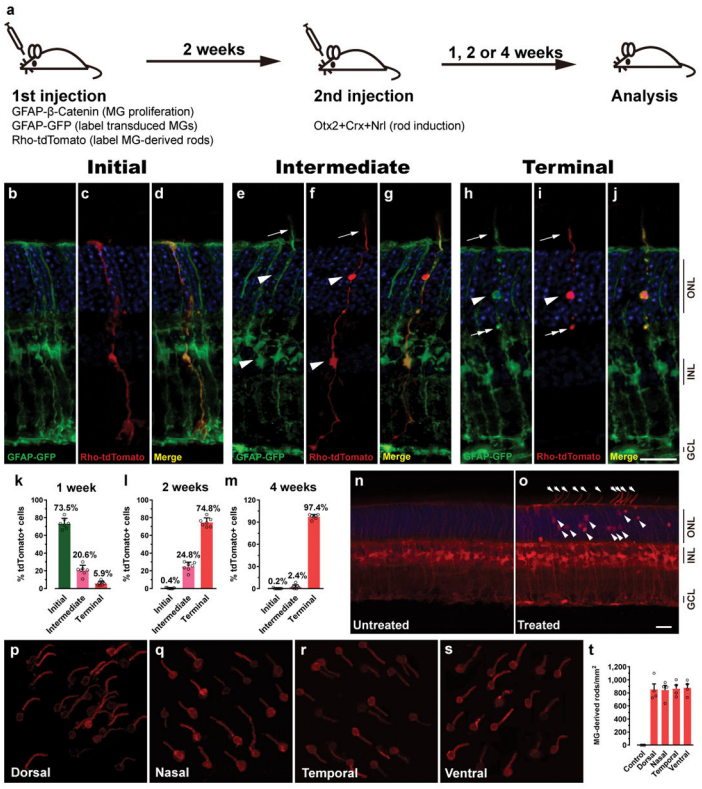

Figure 1. Generation of rod photoreceptors via reprogramming Müller glial cells (MGs) in the mouse retina

a, Schematic illustration of the two-step reprogramming method to generate rod photoreceptors. **b–j,** Characterization of MG-derived rod differentiation through Initial (**b–d**), Intermediate (**e–g**), and Terminal (**h–j**) stages. Arrowheads: cell soma. Arrows: rod outer segments. Double arrows: synaptic terminals. Scale bar: 25 μm. Experiments were repeated 6 times independently with similar results. **k–m,** Quantification of MG-derived rod differentiation at 1 (**k**), 2 (**l**), and 4 weeks (**m**) after the second injection of ShH10-GFAP-mediated gene transfer of *Otx2*, *Crx*, and *Nrl* for rod induction. Data are presented as mean ± SEM, n = 7 retinas. **n and o,** Lineage analysis of MG-derived rod photoreceptors. (**n**) Untreated MG fate mapping mice with MGs labeled by tdTomato. (**o**) Treated MG fate mapping mice using the two-step reprogramming method. Arrowheads: rod soma. Arrows: rod outer segments. Scale bar: 20 μm. Experiments were repeated 4 times independently with similar results. **p–t,** Quantification of MG-derived rod photoreceptors in the Dorsal (**p**), Nasal (**q**), Temporal (**r**), and Ventral (**s**) quadrants of retinal flat-mount preparations at 4 weeks after the second injection for rod induction. Scale bar: 20 μm. Experiments were repeated 4 times independently with similar results. Data in (t) show mean ± SEM, n = 4 retinas. Control measurements were combined across quadrants.

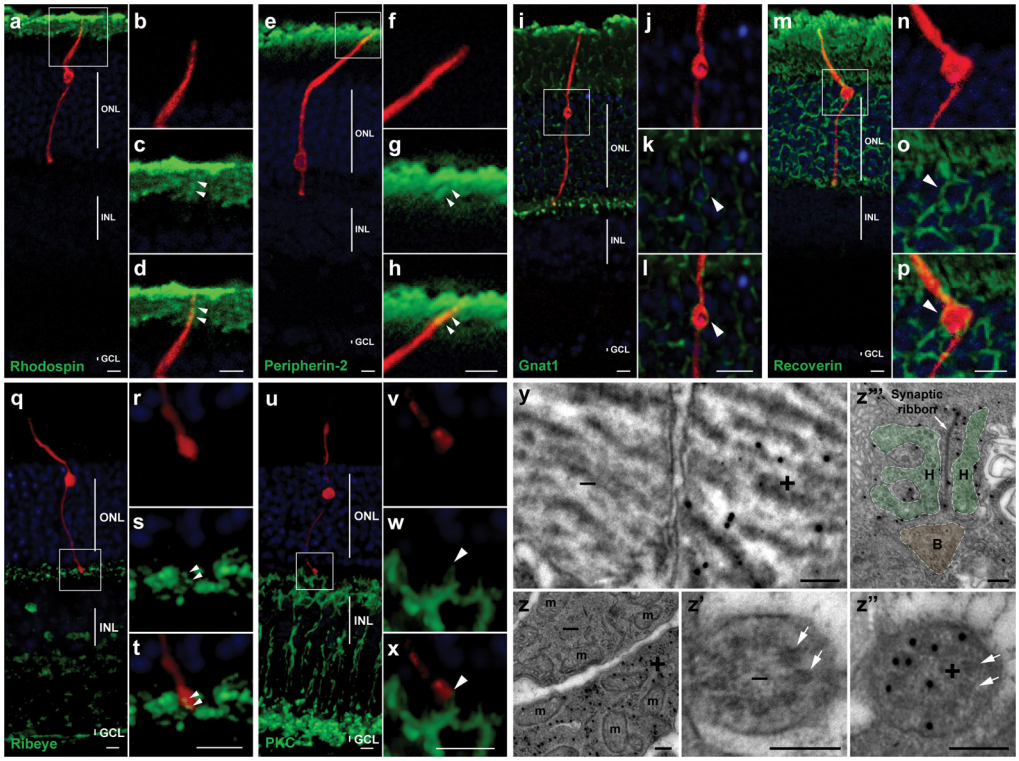

Figure 2. MG-derived rod photoreceptors express essential rod genes and are morphologically similar to native rod photoreceptors

a–t, MG-derived rods (red) correctly expressed a set of essential rod genes (green), including Rhodopsin (**a–d**), Peripherin-2 (**e–h**), Gnat1 (**i–l**), Recoverin (**m–p**), and Ribeye (**q–t**). Arrowheads indicate detection of immunoreactivity in MG-derived rods. **u–x,** MG-derived rods (red) had an enlarged bouton-like synaptic terminal in close apposition (arrowhead) to the PKCα^{+} rod bipolar cells (green). Scale bars: 20 μm (**a, e, i, m, q, u**); 10 μm (**b–d, f–h, j–l, n–p**); 5 μm (r–t, v–x). **y–z‴,** Ultrastructural analysis of MG-derived rods using transmission electron microscopy indicates correct formation of rod outer segments containing densely packed membrane discs (**y**), rod inner segments containing long thin mitochondria (**z**), connecting cilium with microtubule doublets (arrowheads) arranged in a circle (**z′, z″**), and classic triad synapse with horizontal cell axon terminals (letter H in green) and bipolar cell dendritic terminal (letter B in brown) (**z‴**). +, immunogold-labeled MG-derived rods. −, native rods. m, mitochondrion. Scale bar: 200 nm. Experiments were repeated 3 times independently with similar results.

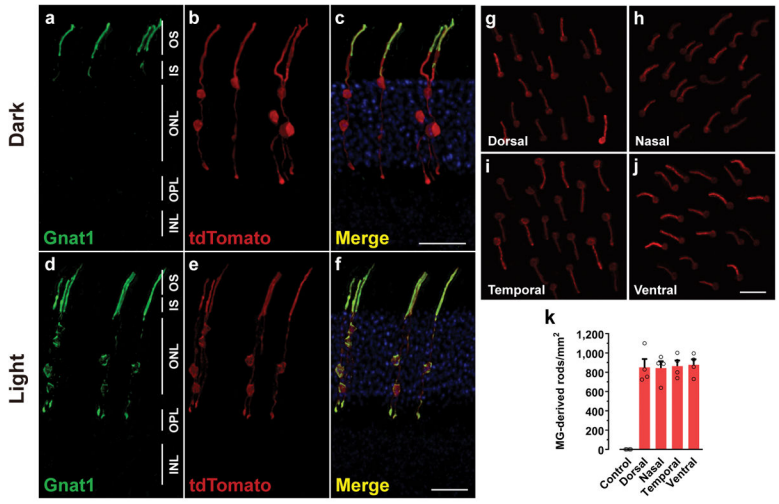

Figure 3. MG-derived regeneration of rod photoreceptors in *Gnat1*^{rd17} *Gnat2*^{cpfl3} mice.

a–f, Gnat1, detected by immunohistochemistry in Rhodopsin-tdTomato^{+} MG-derived rods (**b, e**), translocated from the rod outer segments in the dark-adapted retina (**a–c**) to the rod inner segments, rod soma, and synaptic terminals (**d–f**) upon light stimulation. Experiments were performed 4 weeks after the second injection for rod induction in *Gnat1*^{rd17}:*Gnat2*^{cpfl3} mice. Experiments were repeated 3 times independently with similar results. **g–k,** Effective generation of MG-derived rod photoreceptors in *Gnat1*^{rd17}:*Gnat2*^{cpfl3} mice, analyzed by scoring the number of Rhodopsin-tdTomato^{+} MG-derived rods per mm^2 (**k**) in the Dorsal (**g**), Nasal (**h**), Temporal (**i**), and Ventral (**j**) quadrants in retinal flat-mount preparations. Experiments were repeated 4 times independently with similar results. Scale bar: 20 μm. Data in (**k**) are presented as mean ± SEM, n = 4 retinas.

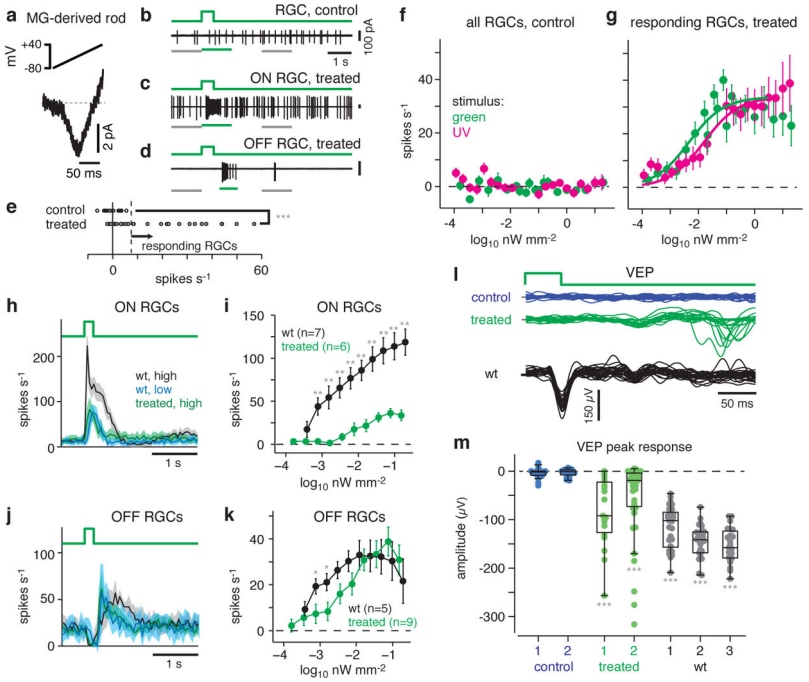

Figure 4. MG-derived rod photoreceptors integrate into retinal circuitry and restore visual function in *Gnat1*^{rd17} *Gnat2*^{cpfl3} mice.

a. Averaged whole-cell current of MG-derived rods (11 recordings; 6 rods, 3 retinas) to a voltage ramp (−80 to +40 mV, 120 ms) shows evidence of Ca^{2+} current. **b–d** RGC spikes to green light (1.0-mm diameter; 1.3/−1.4 $\log_{10}$ nW mm^{-2} in control/treated cell) in response window (green line) relative to baseline windows (gray lines) showed either ON- (c) or OFF-center (d) polarity in treated retinas. **e**, Firing rates to green light (−1.7 to −0.7 $\log_{10}$ nW mm^{-2}) were higher in treated retina (26 cells; 10 retinas, 6 animals) relative to control retina (17 cells; 7 retinas, 4 animals) (***, $p = 2.7 \times 10^{-4}$, two-sided t-test). Responsive cells (n = 15) are those to the right of the dashed line. **f–g**, Average response (±SEM across cells) of RGCs from control (n = 11/17 cells tested at a dim/bright range) and treated retinas (n = 14/9 cells) with fitted sigmoids (see Experimental Procedures). **h,** Post-stimulus time histogram for ON-center RGC responses in treated (6 cells) and wild-type (wt; C57BL/6 strain) animals (7 cells), at either high (−1.7 to −0.7 $\log_{10}$ nW mm^{-2}) or low intensities (−3.8 to −3.4 $\log_{10}$ nW mm^{-2}). (mean±SEM across cells). **i**, ON RGC responses (mean ±SEM across cells) were greater in wt relative to treated animals (**, $p < 0.002$, one-sided t-tests; not adjusted for multiple comparisons). **j**, Same format as (h) for OFF-center RGCs from treated (9 cells) and wt animals (5 cells). **k**, Same format as (i) for OFF-center RGCs (*, $p < 0.05$, one-sided t-tests). **l**, Visually-evoked potentials (VEPs) to a light flash (~3.2 $\log_{10}$ nW mm^{-2}, 50 ms) in primary visual cortex in *Gnat1*^{rd17}:*Gnat2*^{cpfl3} mice of treatment (treated), sham (control) and wt groups. Responses across trials from a single animal are shown, with additional animals in m. **m**, Response amplitude (VEP minimum) for control (2 animals), treated (2 animals) and wt groups (3 animals). Points represent single trials. Box plots show median±interquartile range; error bars indicate full range (minus outliers). All

treated and wt animals showed significant responses (i.e., median different from zero; ***, $p < 0.001$, Wilcoxin signed-rank test), whereas control mice did not.